

Nansen Environmental and Remote Sensing Center

*A non-profit
Research institute affiliated
With the University of
Bergen*



*Thormøhlensgate 47
N-5006 Bergen,
Norway
<http://www.nersc.no>*

NERSC Technical Report no. 297


Solid ice fluxes from the Greenland Ice Sheet



The Petermann Glacier North Greenland in April 2002. <http://environment.newscientist.com/article/>

*Authors:
Mohamed Babiker, Martin W. Miles, Ola M. Johannessen
and Stein Sandven*

Bergen, January 2008

	<p>Nansen Environmental and Remote Sensing Center (NERSC) Thormøhlensgate 47 N-5007 Bergen, Norway Phone: + 47 55 20 58 00 Fax: + 47 55 20 58 01 E-Mail: administrasjon@nersc.no http://www.nersc.no</p>
---	--

<p>TITLE Mass balance and freshwater contribution of the Greenland ice sheet: a combined modelling and observational approach</p>	<p>REPORT IDENTIFICATION NERSC Technical Report no. 297</p>
<p>CLIENT Norwegian Research Council</p>	<p>CONTRACT Project No. 169930</p>
<p>CLIENT REFERENCE</p>	<p>AVAILABILITY Open</p>
<p>INVESTIGATORS Mohamed Babiker, Martin Miles, Ola M. Johannessen and Stein Sandven</p>	<p>AUTHORISATION Bergen, January 2008 Ola M. Johannessen</p>
<p>EXECUTIVE SUMMARY</p> <p>The outlet glaciers of Greenland can drain large volumes of solid ice, via calving of icebergs and bottom melting from floating ice tongues. The contribution of these solid-ice fluxes is controlled by ice dynamics, such that it had been generally believed to have a relatively slow response to climate forcing or changes in boundary conditions. However, this assumption has recently been questioned and observations of one surging glaciers in Greenland suggest relatively large and rapid changes in flux are possible. The magnitude of solid ice entering the ocean can be determined ideally by deriving the ice flux crossing line of calving glaciers, using remote-sensing data and ancillary data. Here, our research goal here is to identify the spatial-temporal variability and possible trends in indicators of calving fluxes for the Petermann glacier in northern Greenland, which is relatively unknown. The methodology approach is based primarily on analysis of repetitive satellite data over a period starting from 1990, together with sporadic earlier observations. Different satellite image data has been acquired and explored to estimate the interannual to decadal mean and variability of frontal position and ice-surface velocity (indicators of solid ice fluxes). The multi-sensor data range from high-resolution optical images from declassified satellite data, Landsat, SPOT and Terra</p>	

ASTER and high-resolution SAR images from ERS and ENVISAT. The SAR data are useful to readily delineate the calving front, regardless of cloud cover. The SAR data include ERS-1/-2, and ASAR ENVISAT. These disparate data have been imported, geo-registered and analysed within a Geographic Information System. Two analysis methods have been used: 1) Delineating the calving front of the glacier and 2) Estimating the surface velocity using sequential satellite images. We have found from our decadal+ series of image measurements, the surface velocity of the Petermann glacier, below the grounding line is around 800 m per year in early 1990s and slightly greater than 1 km per year in 2002. The calving-front position variability is more episodic, with two main mass discharges from the glacier to the open water in 1991 and 2001.

Contents

1. Background	2
2. Solid Ice Fluxes	2
3. Satellite data	3
3.1 OPTICAL IMAGES	4
3.2 SAR IMAGES	6
4. Methods	8
5. Petermann Glacier	9
6. Nioghalvfjærdsfjorden Glacier	14
7. References	18

1. Background

There is unequivocal evidence for rapid and large climate variations in the Northern Hemisphere during the last glacial [Stocker, 2000]. These fluctuations involve major changes in few decades, and probably associated with the shutdown of the thermohaline circulation (THC) in response to massive iceberg discharge events from the Laurentide ice sheet, resulting in a freshening of the surface waters in the North Atlantic. Changes in the north Atlantic THC in response to small changes in the hydrological cycle, for instance variability in the outflow of Eurasian rivers or meltwater from Greenland ice sheet, (GrIS) have also been implied as causing rapid climate change [Ganapolski and Rahmstorf, 2002]. The GrIS is the largest single freshwater sources in the Northern Hemisphere, containing enough water to rise global sea level by about 7 m.

A likely consequence of global warming is partial melting of GrIS, resulting in an increased freshwater flux into the surrounding ocean that could perturb the THC. Freshwater sensitivity experiments in some ocean and climate models predict a critical additional freshwater flux entering the northern Atlantic between 0.06 and 0.15 Sv ($1 \text{ Sv} = 10^6 \text{ m}^3 \text{ s}^{-1}$) after which the THC cannot be sustained [Rahmstorf, 1995]. At present, the GrIS contributes an estimated annual freshwater flux of 0.00031 Sv through ablation and calving of icebergs. This present-day flux is relatively small but non-negligible when compared to the discharge of the six largest Eurasian rivers (0.06 Sv). For the GrIS, the sensitivity of ablation and subsequent runoff is estimated to be $0.0018 \text{ Sv } ^\circ\text{C}^{-1}$ (local temperature) [Van de Wal et al., 2001]. On centennial timescale, coupled climate-ice dynamical models project that half of the GrIS could disappear by the year 2500 [Huybrechts and De Wolde, 1999], corresponding to an additional freshwater flux of 0.1 Sv.

Recent results from coupled Atmosphere-Ocean Global Circulation Models (AOGCMS) have indicated that the additional freshwater from Greenland may cause the THC to shut down by the end of this century, resulting in a sharp cooling of the North Atlantic region [Fichefet et al., 2003]. Moreover, the modelled annual freshwater fluxes from GrIS show extreme interannual variability with a typical standard deviations close to 100% of the mean value [Huybrechts et al., 2002]. The magnitude, timing and spatial distribution of these ablation peaks can be of great importance for a system as sensitive as the north Atlantic deep water formation, yet no climatological data of freshwater fluxes from the ice sheet exist. High resolution regional ocean models of Arctic, consequently, generally ignore this significant sources of freshwater even though it is currently similar in magnitude to river runoff (and likely to greatly exceed it in the future) [Maslowski et al., 2000].

2. Solid Ice Fluxes

The mass loss from the Greenland ice sheet (GrIS) composes of melt-water and solid ice. The outlet glaciers of Greenland can drain large volumes of solid ice, lost via calving of icebergs and bottom melting from floating ice tongues. The contribution of these solid-ice fluxes is controlled by ice dynamics, such that it had been generally believed to have a relatively slow response (thousands of years) to climate forcing or changes in boundary condition. However, this assumption has recently questioned [Zwally et al., 2002], in addition observations of on surging glacier in northern Greenland suggest relatively large and rapid changes in flux are possible [Joughin et al., 1996], though neither the dynamics nor variability of these fast glaciers are well understood.

The magnitude of the solid ice entering the ocean from the Greenland Ice Sheet can be determined by deriving the ice flux crossing the grounding line of calving glaciers, using interferometric synthetic aperture radar (InSAR) and ancillary data. This has been undertaken by Rignot et al. [1997 and 2001] for most of the glaciers in northern Greenland and these results serve as the initial benchmark for solid ice fluxes from this part of GrIS, towards our research goal

of identifying the spatial-temporal variability and possible trends in calving fluxes, which are relatively unknown. The methodological approach had been observational, based primarily on analysis of repetitive satellite data (radar and optical) over a period of time, starting from 1991 till present.

First, an intensive search of data had been conducted to develop a decadal-scale dataset of major glaciers in northern Greenland. Whereas most Greenland outlet glaciers flow directly into the ocean, in northern Greenland, most have floating tongues. The target areas include the major ones in the N/NW sector – Humboldt, Petermann, Ryder, Ostensfeld – and NE – Nioghalvjerbrae, Zachariae Isstrøm and Storstrømmen (Fig 1). This extensive geographical coverage is important, as these control most of the ice discharge in northern Greenland and because surveys have indicated very large glacier to glacier differences in mass budgets, including the proportion of loss through calving and basal melting.

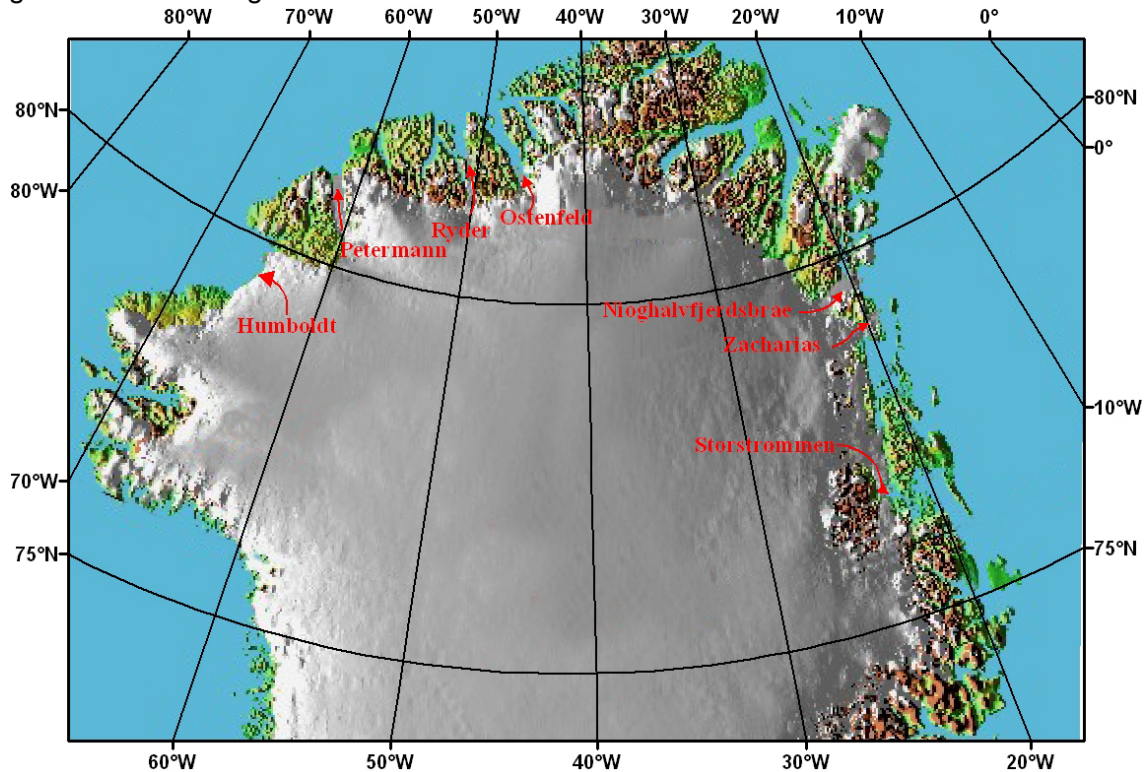


Figure 1. Map of North Greenland shows the investigated glaciers.

Second, SAR and visible-band satellite data has been analysed for mapping calving-front features. In principle, calving of icebergs should be detectable down to the resolution of the sensor. However, quantitative retrieval of icebergs is not straightforward, as automatic methods for differentiating icebergs from the surrounding ocean/sea-ice matrix are not adequately consistent. Also, the intra seasonal variability and possible trends in location has been identified of calving front.

Third, the annual surface velocity of some glaciers has been determined by using sequential satellite images.

3. Satellite data

The data include main types of satellite images: high-resolution optical images from declassified Satellite imagery, Landsat, SPOT and Terra ASTER, and high-resolution SAR images from ERS and ENVISAT. Selections of these data were collected for the Northern Greenland glaciers and are presented in this report. The satellite dates is up to data in order to detect changes in the most recent years, when condition may be changing, particularly in summer.

Due to the amount and coast of the data only quick looks were downloaded in addition to some free data available for download (landsat) since there is no money allocated for buying data in the project budgeted. The quick look can be used for delineating glacier front, but due to low resolution it cannot be used from displacement measures.

3.1 Optical images

Declassified Satellite Imagery

Declassified imagery consists of two groups: declassified Satellite Imagery – 1; Include photographic images that were taken between 1959 and 1972. These images were primarily collected by the CORONA satellite series, but the dataset also includes photos taken from the ARGON and LANYARD satellites. Declassified Satellite Imagery – 2; include images that were taken from 1963 to 1980. These photographic images were collected by the KH-7 Surveillance System and the KH-9 Mapping System (Fig. 2). The images have variable scales and the image quality can be variable. Cloud cover is common.

All Declassified Satellite Imagery can be searched and ordered through Earth Explorer; preview is available online for all images prior to purchase. The price for high-resolution scanned image is \$30.00 per frame. Products from KH-7 are vary in length, ranging from 4 inches to 500 feet. Prices are determined according to the number of 30-inch segments that occur within a particular image. The numbers of segments per image are identified when searching and ordering.

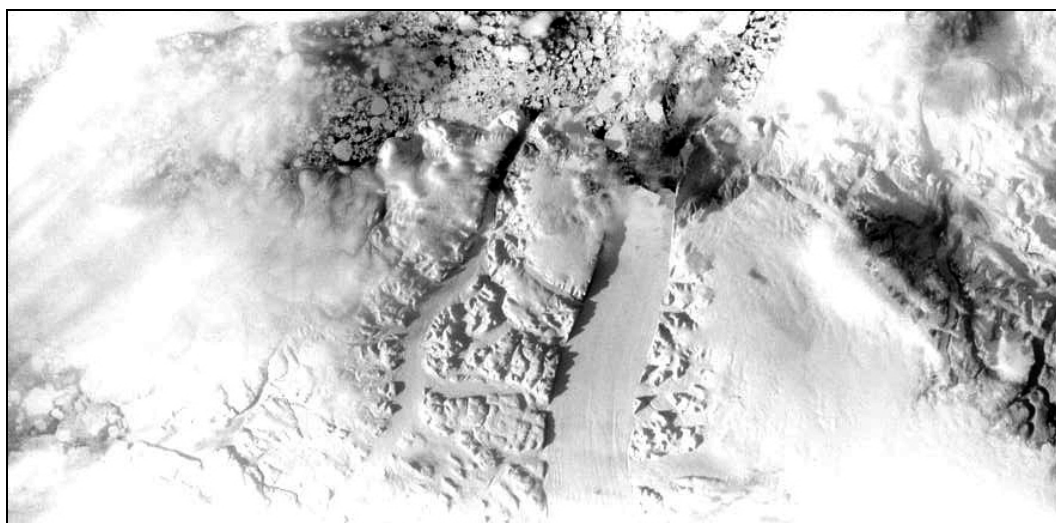


Figure 2. KH-9 black and white quicklook image from 20 September 1977 covering Pertermann glacier.

Landsat

Landsat represents the world's longest continuously acquired collection of space based and remote sensing data. The first landsat satellite was launched in 1972; the most recent, Landsat 7 was launched April 15, 1999. The table below summarizes the main characteristics for the landsat imagery.

Satellite	Start	End	Sensor	Resolution (metre)	Swathwidth
<i>Landsat 1</i>	July 72	January 78	RBV, MSS	80, 79	185 km
<i>Landsat 2</i>	January 75	February 82	RBV, MSS	80, 79	185 km
<i>Landsat 3</i>	March 78	March 83	RBV, MSS	40, 79	185 km
<i>Landsat 4</i>	July 82	August 93	MSS, TM	82, 30	185 km
<i>Landsat 5</i>	March 84	Running	MSS, TM	82, 30	185 km
<i>Landsat 6</i>	October 93	Failed			
<i>Landsat 7</i>	April 99	Running	+ETM	30 (ms), 15 (pan)	185 km

There are a good number of landsat scenes covering the north part of Greenland that extend to about 81°30' north (the approximate northern limit of the Landsat orbits). As the other optical sensors the common problem is the cloud cover and the difficulty in differentiate between cloud and snow. Images are available for this area is mainly in summer period and that is due to sun angle. When Landsat images have been acquired, a quicklook version can be browsed and downloaded to check if the quality of the image before full-resolution image can be ordered. An example of a quicklook Landsat image is shown in Fig. 3,A covering the Storstrømmen Glacier on 18 August 1973 and B covering Humboldt Glacier on 14 August 1987. The quicklook images show the calving fronts of the glacier and some sea ice and iceberg. There are a limited number of full resolution images are available for free to download, all images covering the study area were downloaded and added to the database of the project.

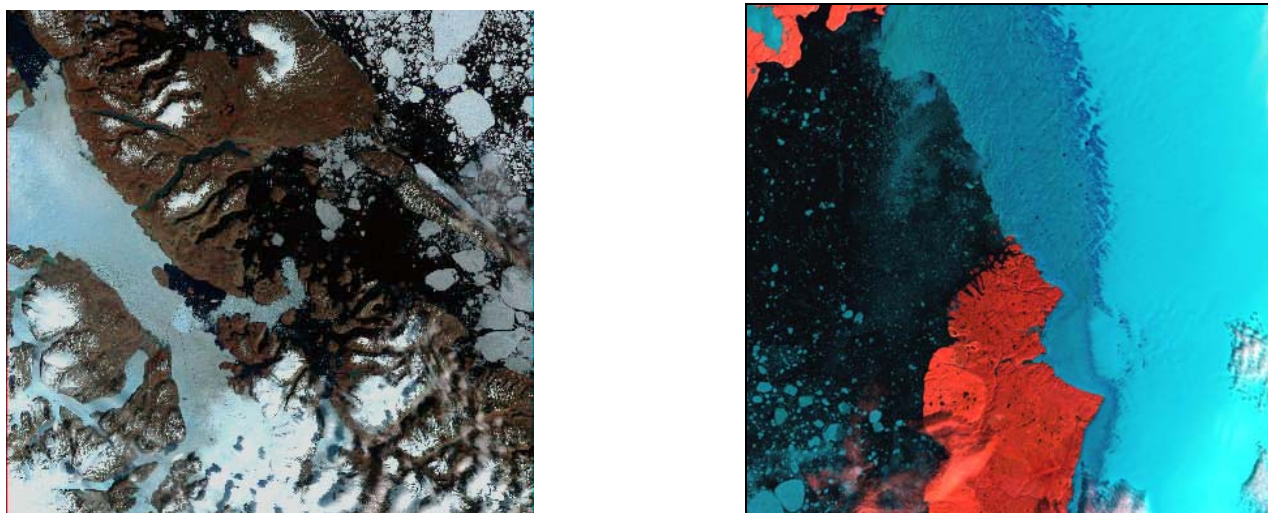


Figure 3.(A) Landsat MSS quicklook image from 18 August 1973 covering the Storstrømmen Glacier.(B) Landsat Tm image from 14 August 1987 covering Humboldt Glacier.

SPOT

SPOT, (Earth Observation System) began operations in 1986 with launch SPOT1, and was conceived and designed by France with cooperation of other European countries. The table below summarizes the main characteristics of the SPOT system.

Satellite	Start	End	Resolution	Coverage
SPOT1	February 1986	December 1990	20 (ms) 10 (pan)	60X60 km
SPOT2	January 1990	Still operational	20 (ms) 10 (pan)	60X60 km
SPOT3	September 1993	November 1997	20 (ms) 10 (pan)	60X60 km
SPOT4	March 1998	Still operational	20 (ms) 10 (pan)	60X60 km
SPOT5	May 2002	Still operational	10 (ms) 5 & 2.5 (pan)	60X60 km

SPOT can offer the best quality and coverage of high-resolution optical images in any areas of the world. There are three satellites are in operation with steerable antennas to map areas on request from customers. This makes it possible to have more frequent coverage of a given area compared to Landsat and ASTER. The disadvantage of the SPOT image for a project like this is prices since huge data is needed; it is expensive compared with other satellite. SPOT has a good coverage from north Greenland especially in the nineties. A quicklooks are available from SPOTImage, they can be browsed and downloaded to check if the quality of the image before full-resolution image can be ordered. Here, some quicklooks has been downloaded to study the calving front for some glaciers (Fig. 4). Studying surface velocity is not possible due the low resolution of the quicklook.

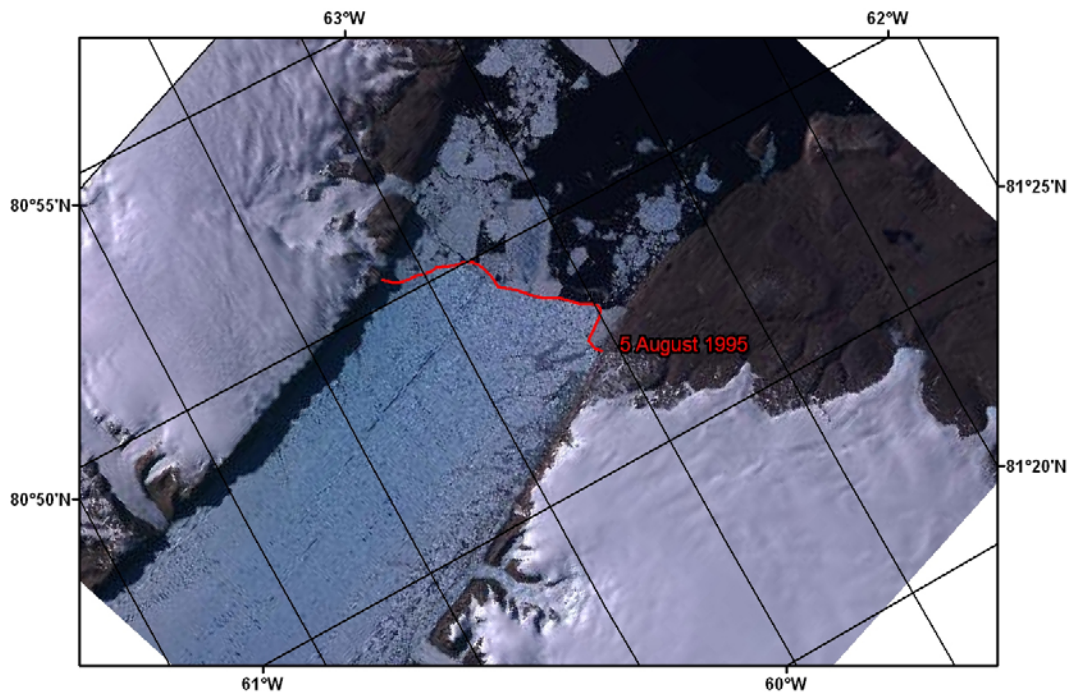


Figure 4. SPOT quicklook image from 5 August 1995 covering Petermann glacier, the calving front of the glacier is delineated.

Terra ASTER

ASTER (Advanced Spaceborne Thermal Emission and Reflection Radiometer) is an imaging instrument flying on Terra, a satellite launched in December 1999. It is an imaging radiometer designed to collect data in 14 spectral channels. Three channels in the visible and near infrared provide 15-m resolution; six channels in the short wave infrared provide 30-m resolution and five channels in thermal infrared provide 90 resolution. The image coverage is 60X60 km.

ASTER has been used intensively for studying glaciers worldwide through the Global Land Ice Measurements from Space (GLIMS) project. The project designed to monitor the world's glaciers primarily using data from optical satellite instruments, such as ASTER. GLIMS began as an ASTER Science Team project. Through this connection, they have guided the ASTER instrument to acquire imagery of Earth's glaciers that is optimized (best season and instrument gain settings) for glacier monitoring. Free images from ASTER are available for the GLIMS network partners, contact has been made to get images for this project through GLIMS but with no success.

Only three ASTER images were available in full resolution to this project, which received from another project, the rest are quicklook images (Fig. 5).

3.2 SAR images

The data of SAR images include European Remote Sensing satellites (ERS), ASAR ENVISTA and ALOS data. These data were received free of charge from ESA after our International Polar Year (IPY) AO proposal was accepted this year. The data include the following:

- 100 ENVISAT ASAR archived products (on demand production)
- 200 ERS SAR archived products (on demand production)
- 50 ERS SAR new products (on demand acquisition and production)
- 40 ALOS PALSAR archived products (on demand production)
- 10 ALOS PALSAR new products (on demand acquisition and production)

SAR images are the most common images used for glaciers studies that due to their capability of penetrating clouds and

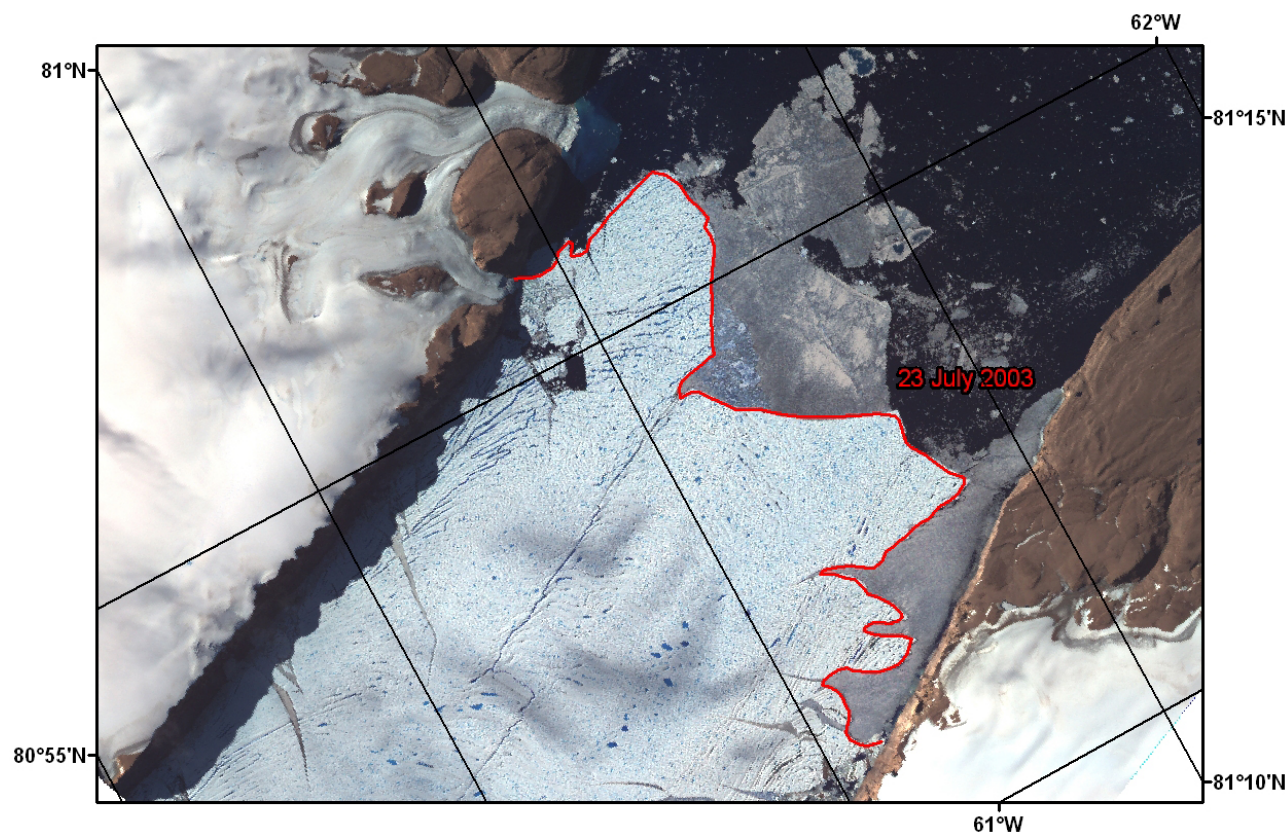


Figure 5. ASTER image from 23 July 2003 covering Petermann glacier, the calving front of the glacier is delineated.

ERS 1&2

The European Space Agency (ESA) launched its first remote sensing satellite ERS-1 on July 1991 in sun-synchronous orbit at inclination of 98.5° . ERS-1 carries three principle sensors (1) a C-band active microwave instrument (AMI), (2) a *Ku*-band radar altimeter (a nadir looking instrument for altitude measurements) and (3) a long track scanning radiometer (a passive instrument consisting of an infrared radiometer and a microwave sounder). ERS-2 was launched on April 1995. Largely identical to ERS-1, it added additional instruments and included improvements to existing instruments including: GOME (Global Ozone Monitoring Experiment) and ATSR-2 included 3 visible spectrum bands specialized for Chlorophyll and Vegetation. When ERS-2 was launched, ERS-1 shared the same orbital plane. This allowed a tandem mission, with ERS-2 passing the same point on the ground 1 day later than ERS-1. The images used in this project are mainly coming from the (AMI), which can operate in one of three modes: IMAGE, WAVE or WIND (only one of these can be used at any given time). In the IMAGE mode, the AMI produces SAR data over a 100-km swath at a resolution of approximately 25 m with VV polarization at a 23° look angle. ERS satellites acquire data in ascending and descending passes that provide SAR coverage up to 82°N .

ENVISAT ASAR

ENVISAT was launched in March 2002; in addition to the other instruments it carries the Advance SAR (ASAR) instrument. The ASAR, operate at C-band can be regarded as an advance version of the SAR instruments on board the ERS1 and ERS2 satellites. Its beam elevation steering allow the selection of different swaths at different incident angle, providing a swath coverage of 100km for Image and alternating polarization modes, 5km for wave mode and 400km or more for wide swath and global monitoring modes. In the image mode, which is used in this project, ASAR operates in one of seven predetermined swath (100km) with either vertically or horizontal polarized radiation

the same polarization is used for transmit and receive (i.e., HH or VV). The ground resolution is about 30 m, sampled at pixel separation of 12.5 m. In the alternating polarization mode (in one of seven possible swaths), two images in two polarization modes (HH & VV, or HH & HV, or VV & VH) are acquired. The ground resolution is about 30 m, sampled at 12.5 m spacing. When operating in the wide swath mode, a wide swath of > 400 km can be achieved, at a ground resolution of about 150 m, sampled at 75 m pixel spacing. When using a wide swath image for studying glaciers, it is possible to delineate the calving front in the summer season (Fig. 6).

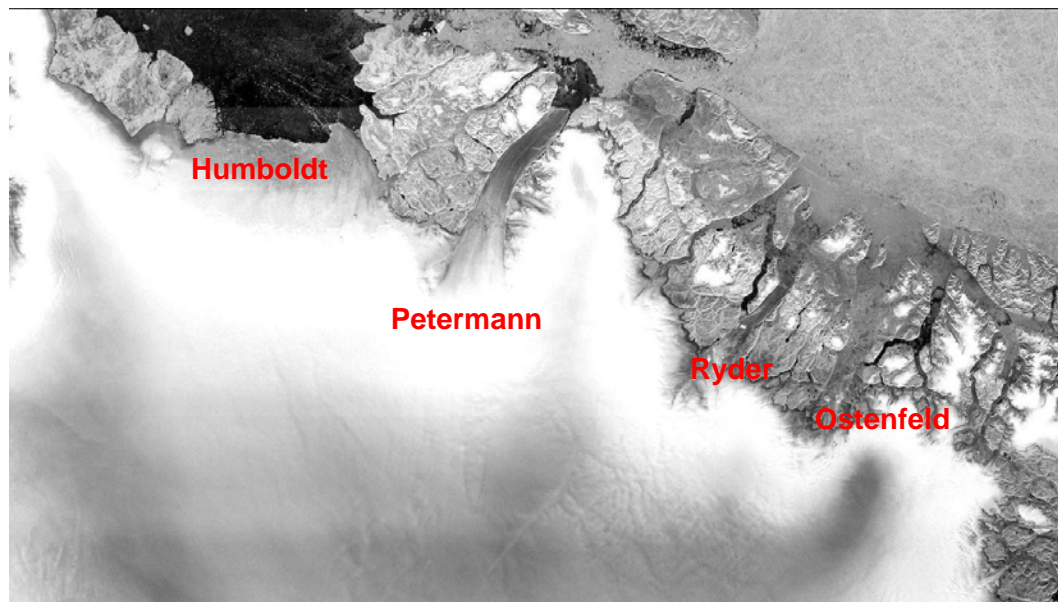


Figure 6. A wide swath ASAR quicklook image from 21 September 2007 covering the north part of Greenland where the main glaciers are indicated.

4. Methods

The image data have been imported, geo-registered and analysed within the Geographic Information System ArcGIS. Two analysis methods have been used here: 1) delineating the calving front of the glaciers and 2) estimating the surface velocity of the glaciers using sequential satellite images. Delineating the calving front of the glacier is a straightforward method and it is common for studying the advance and retreat of the glaciers, as has been used with maps, photos and satellite images. The only difficulty sometimes the differentiation between the calving front and the sea ice, especially in the winter season.

Numerous techniques have been developed to measure the velocity of ice flow. Early techniques involved conventional surveying methods. Satellite positioning system opened the possibility for repeated positioning of markers on the polar ice sheet where no stationary points are nearby (Whillans *et al.*, 1987). Photogrammetric methods have been applied to aerial photographs or high-resolution satellite imagery. This technique relies on a visible features on the glacier surface that can be traced in sequential images or photos (1995; Whillans and Tseng, 1995; Csatho, *et al.*, 1999) However, these methods have been limited to areas where well-defined, fixed points are plentiful enough that multiple photographs or images can be coregistered. Radar interferometry has been applied to measure velocities in Greenland Ice sheet by using the phase information from synthetic aperture radar (SAR) images to determine the surface velocity component in the satellite viewing direction (e.g. Rignot *et al.*, 1997; Rignot and Kanagaratnam, 2006).

Here, we determined velocities by tracking features in images of different years. Cross-correlation method or automated feature-tracking method of grey levels has been used successfully (Bindschadler and Scambos, 1991; Howat *et al.*, 2007); however, this technique requires images of similar radiometry and geometry, which is not the case here, where images from several different sensors (e.g., ERS, Landsat, ASTER and ENVISAT) are used. Therefore, to overcome

these problems, the images were analysed visually. The images used for feature tracking are first geometrically and radiometrically adjusted using ERDAS IMAGINE software to appear as similar as possible. Then a database of the images was created in ArcGIS. Here, the GIS capability of overlying the image on the top of each other and increase the transparency of the top image enabled both images to be viewed simultaneously or in a short sequence. Then the distance between the same feature in the two images was tracked manually and digital vector overlays produced.

5. Petermann Glacier

Petermann Glacier, located at 60° W and 81° N in the northwest Greenland Ice Sheet, is named after the German geographer Dr. A. Petermann. Petermann Glacier is one of the longest glaciers in the northern hemisphere. It develops an extensive floating tongue (70-km long), with a terminus only a few meters above sea level (Rignot 1998). The glacier grounding line is more or less in the same position today (Rignot, 1996). Historical photographs also suggest that little change in the glacier ice front position occurred in the past 50 years (Higgins, 1991).

The table below shows the images used for studying the frontal behavior and velocity measurement for the Petermann Glacier, in addition to other quicklook images from SPOT and ASTER were also used for delineating the front when full resolution images were not available. The images were adjusted coregistered and rectified to the same projection and datum using some fixed points available from the outcrops surrounding the glacier. The images are also radiometrically adjusted to facilitate identification of the same features, and features in the two images were then traced on Arc GIS.

Figure 6 shows the Landsat images from 07 July 1999 covering the front part of the Petermann Glacier overlaid by the glacier front delineated from the other images. There is no clear advancing or retreating of the glacier it is more fluctuation and that may be due to floating tongue of the glacier. There are two clear events of mass discharge from the glacier to the **open ocean**, the first event took place in 1991 (between 12 July and 24 September 1991) as the change in the front shown by the SPOT quicklook image of the 12 July 1991(fig 7a) and the ERS image of the 24 September 1991 (fig 7b). The second event in 2001 and precisely between 17 July 2001 and 21 August 2001 as shown by the front delineated from the ASTER image 17 July 2001(fig 7c) and the SPOT quicklook image from 21 August 2001 (fig 7d). The location of the front for the time been (2007) is the same as between 1998 and 1999. The minimum location reached was in September 1991 and in August 2001 after the discharge events mentioned above. Rignot (1996) suggested that Petermann Glacier loses mass to the ocean mostly through basal melting of its floating tongue, but here we found that also great losses coming from iceberg discharge. The area lost from the above two mentioned events is about 214 km² in 1991 and 71 km² in 2001.

Satellite			
<i>ERS 1 & 2</i>	<i>ENVISAT (IMP)</i>	<i>Landsat</i>	<i>Terra ASTER</i>
24 September 1991	06 August 2004	07 July 1999	17 July 2001
26 April 1992	28 August 2004		20 July 2002
16 September 1992	29 August 2005		23 July 2003
7 March 1993			
27 May 1994			
02 March 1995			
01 March 1996			
21 March 1997			
12 March 1998			

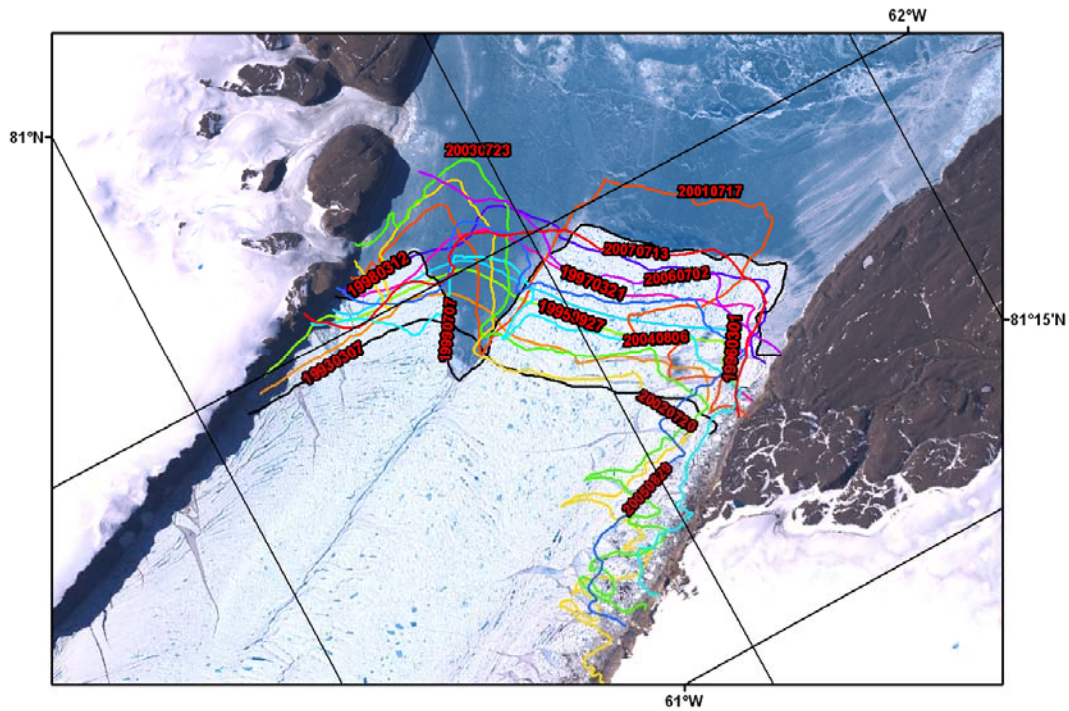


Figure 6. Landsat image from 7 July 1999 covering the front part Petermann Glacier overlaid by the front delineated from the other images used to study the frontal behavior.

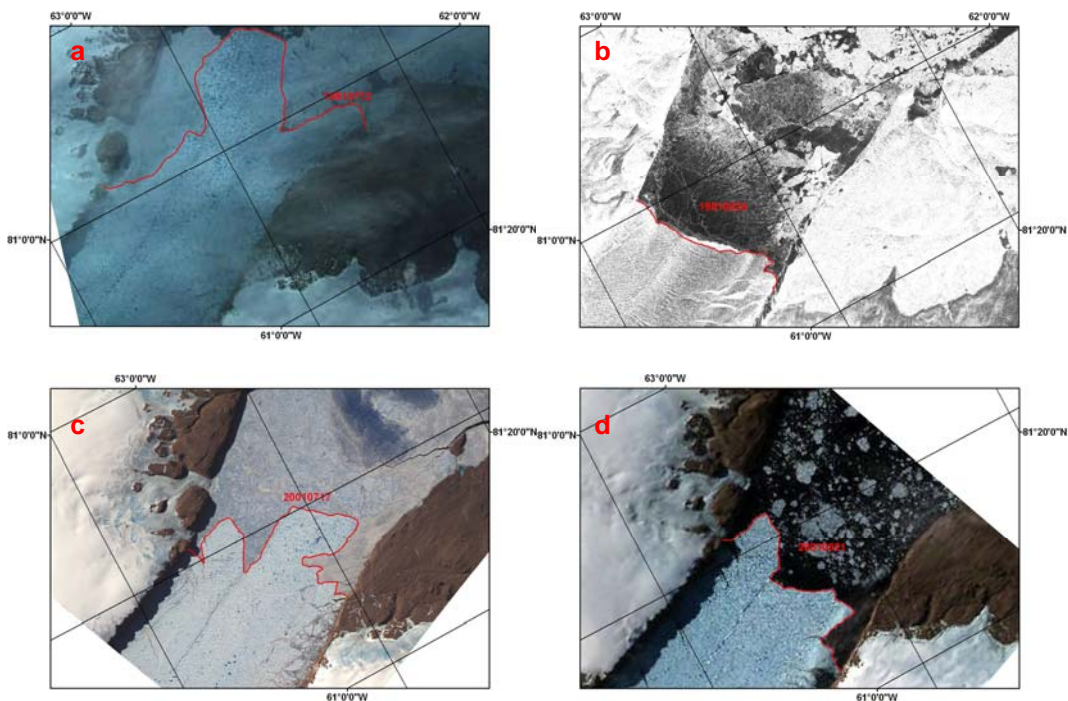


Figure 7. Shows the two major mass discharge from the Petermann Glacier to the open ocean in 1991 the upper images and 2001 the lower image. a) SPOT quicklook image from 12 July 1991, b) ERS image from 24 September 1991, c) ASTER image from 17 July 2001 and d) SPOT quicklook image from 21 August 2001.

The images showed in the table above are the only images used to study the velocity, no quicklook images are used that because the resolution are not good enough to recognize features that can be identified in two images. These images are coming from different sensors that is the

reason it is not easy to apply cross correlation method. The features used for measuring the velocity are easy identified in the optical images (landsat and ASTER) than in the SAR images. Figure 9 shows how these features look in the different sensors.

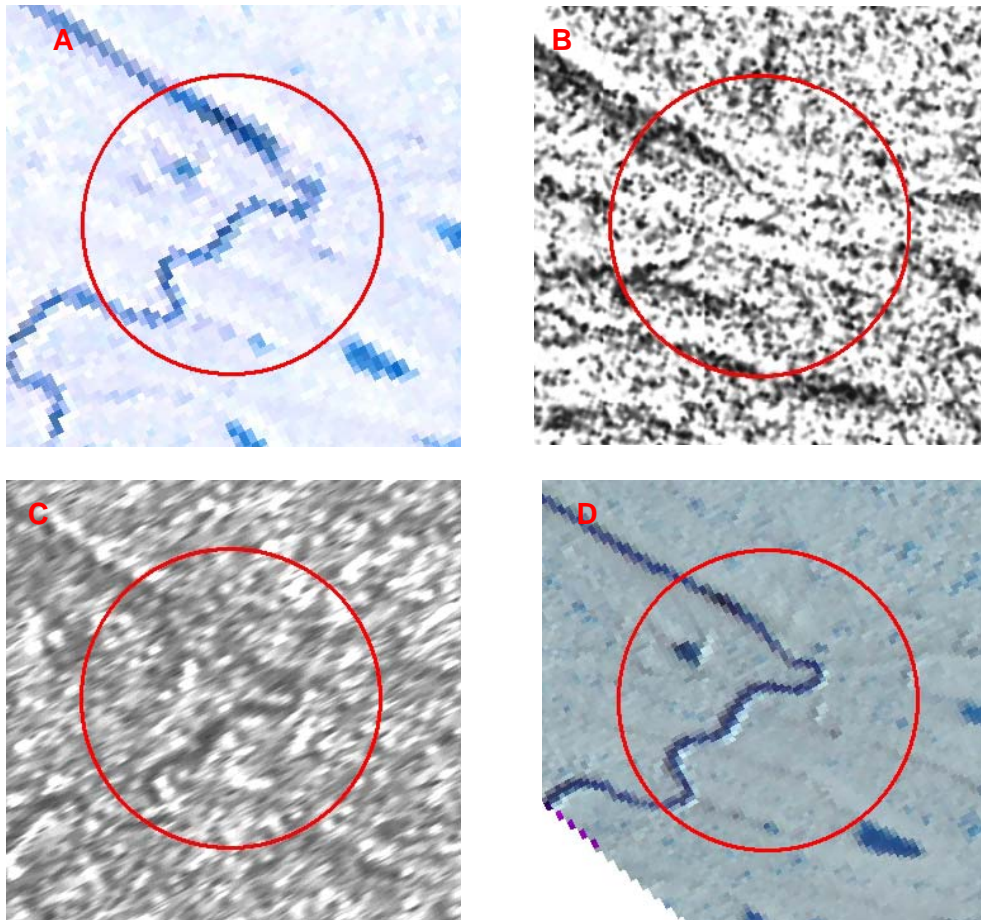


Figure 8. Magnified view of the same feature in four different sensors, A Landsat, B ERS SAR, C ENVISAT ASAR and D ASTER.

Minimum 30 features as the one shown in figure 8 were used and the distances between them were measured in Arc GIS after overlaying each image on top of each other. The output is vector layer representing the velocity of the glacier on the period of the two images. Figure 10 shows an example of the velocity layer; it shows an ASTER image from 20 July 2002 and the vector layer represents the displacement (velocity) from 20 July 2002 to 23 July 2003. The table below summarizes the velocity measured using the available images. The mean was calculated from the each vector layer to represent the period. There was no different in the velocity at different parts of the glacier, a test was conducted to see if there is any differences between e.g. the middle part and the side of the glacier no recognizable differences were found.

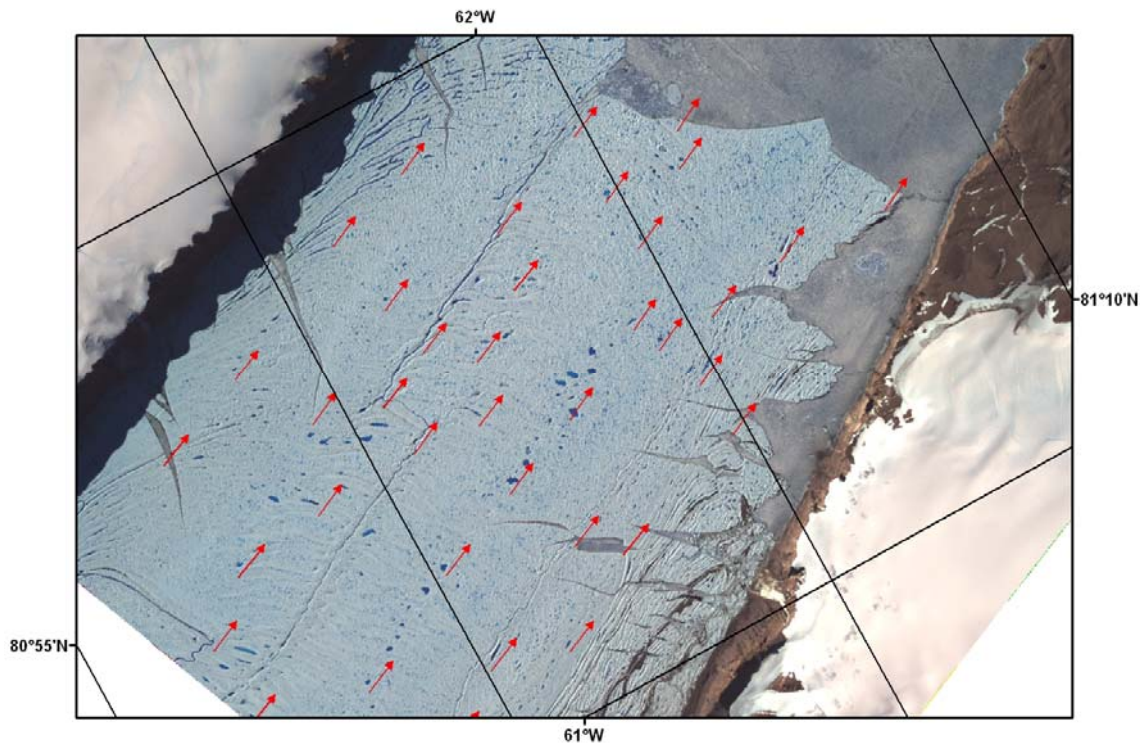


Figure 9. ASTER image from 20 July 2002 and the vector layer represent the displacement (ice surface velocity) from 20 July 2002 to 23 July 2003.

To understand the general trend of the velocity for this period graphs were plotted from the velocity data. Figure 10a shows the velocity between two images in succession, the differences between these images sometimes is more or less than the 12 months, the annual average velocity was calculated and plotted in figure 10b. Figure 10b show slight increase in Petermann glacier velocity in the period from 1991 to 2002. The surface velocity range from 800 m/yr in 1991/1992 to 1111 m/yr 1997/1998.

From	To	Velocity in meter
24 September 1991	26 April 1992	254
24 September 1991	16 September 1992	800
26 April 1992	16 September 1992	439
26 April 1992	7 March 1993	828
7 March 1993	27 May 1994	1198
27 May 1994	2 March 1995	801
27 September 1995	1 March 1996	365
2 March 1995	1 March 1996	927
1 March 1996	21 March 1997	1077
21 March 1997	12 March 1998	1111
12 March 1998	7 July 1999	1426
7 July 1999	17 July 2001	2095
17 July 2001	20 July 2002	1095

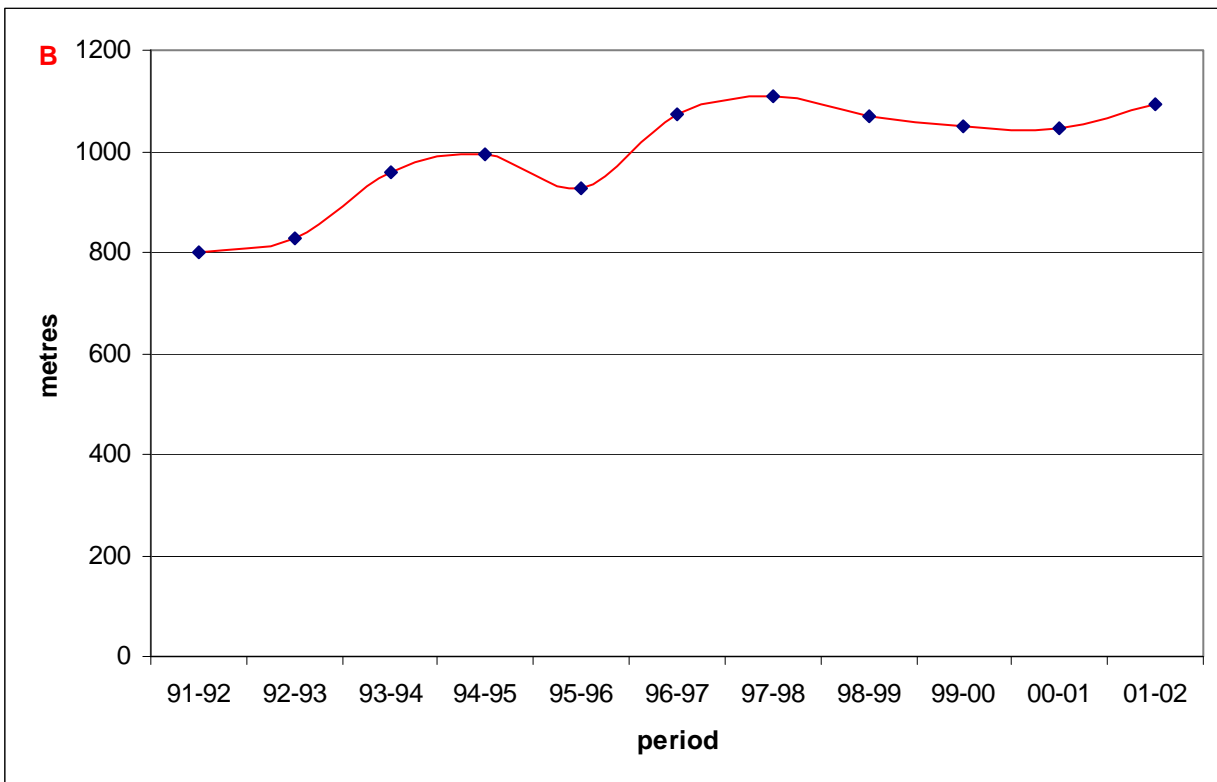
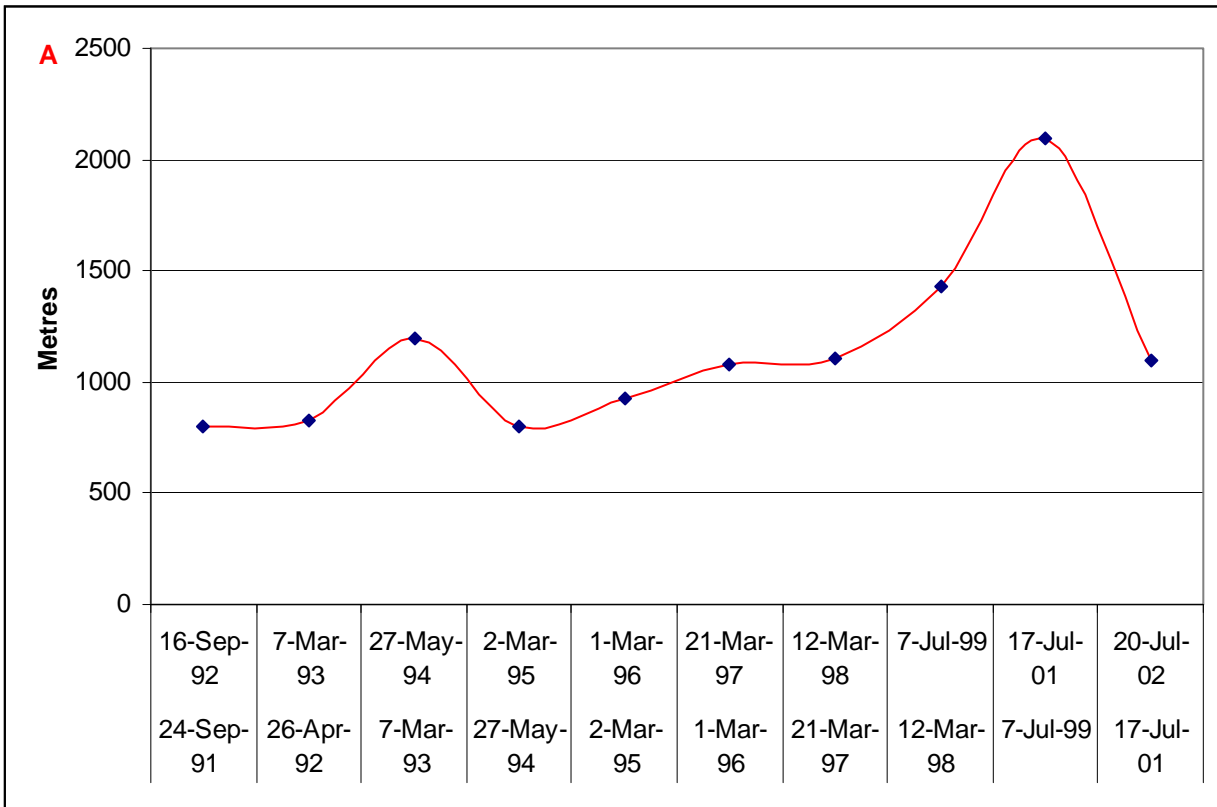


Figure 10. Shows two graphs (A) the measured surface velocity for the Petermann in the period 91-2002, (B) the annual average surface velocity for the same period.

The above estimated surface velocities for Petermann Glacier are comparable with previous studies using different methods. Higgins (1991) estimated the velocity to be 950 m/yr, (Rignot *et al.* 1997) calculating the velocity using Radar interferometry to be 1139 m/yr and (Joughin *et al.* 1999) also applying Radar interferometry found the velocity to be 1100 m/yr.

6. Nioghalvfjærdsfjorden Glacier

Nioghalvfjærdsfjorden Glacier is located 22° W and 79° N, on the northeastern Greenland (fig 1, and 11). This glacier drains ice from the Greenland ice sheet via a large icefall at the west end of the fjord. The glacier tongue is 80 km from the west to east, and 21 km wide halfway along its length, widening to about 30 km at the main ice front. A northern branch of the glacier, 8 km wide drains into the fjord Dijnphna Sund west of Hovagaard Ø (Thomsen *et al.* 1997). The length of the floating tongue is about 60 km with grounding line located at the western branch of the marginal lake Blåso, in which tidal movements have been observed (Thomsen *et al.* 1997). The floating part of the glacier constitutes an extremely flat ice plain. The main ice front of the glacier is split by islands into three, 7-8 km long ice tongues; the ice to tongues have a characteristic saw-tooth lateral margins.

The data used to study the frontal behaviour and the surface velocity for the Nioghalvfjærdsfjorden Glacier are summarized in the table below. The period is from 1992 to 2001.

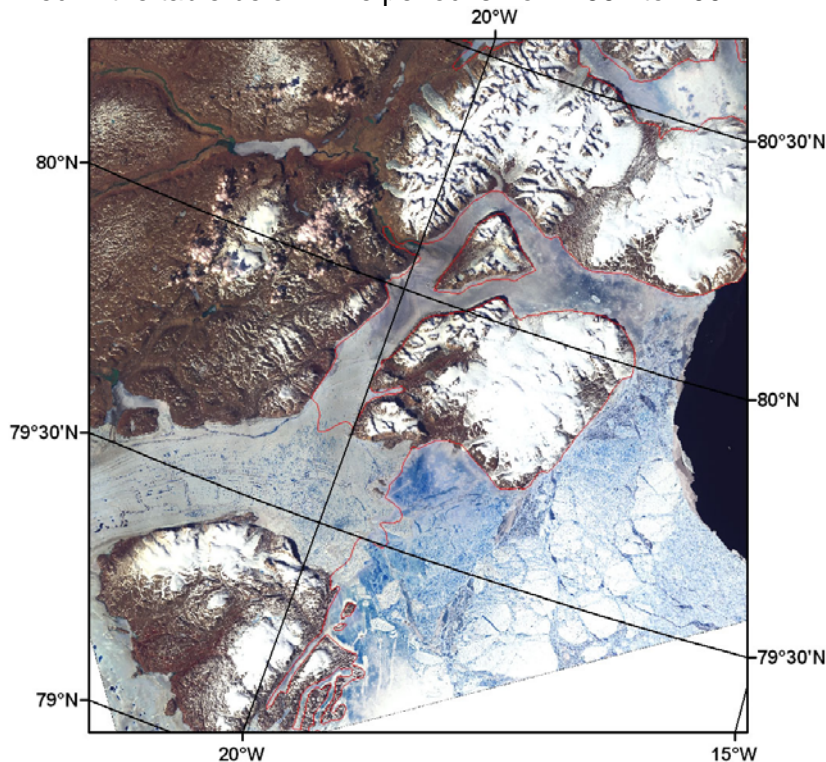


Figure 11. Landsat image from the 26 June 2001 shows Nioghalvfjærdsfjorden Glacier front.

Satellite	
ERS	Landsat
1 March 1992 (ERS1)	Landsat TM 2 July 2000
20 April 1993 (ERS1)	Landsat TM 26 June 2001
9 March 1994 (ERS1)	
13 March 1995 (ERS1)	
12 March 1996 (ERS1)	
27 March 1997 (ERS2)	
31 March 1998 (ERS2)	

The images were adjusted coregistered and rectified to the same projection and datum using some fixed points available from the outcrops surrounding the glacier. The images were also radiometrically adjusted to facilitate identification of features to be used for surface velocity measurement.

All available images and quicklook images have been evaluated to document the glacier front and its behavior, in some cases images it was difficult to identify the glacier front that was due to the presence of sea ice. The images show stable condition for the glacier front (fig 12). Earlier studies concluded the same; Thomsen *and others* (1997) evaluated aerial photographs and landsat quicklook data from 1950 to 1993, they concluded that stable condition at the main glacier front with no major calving events from 1963 to 1993. The stable condition of the front may be due to the presence of a semi permanent sea-ice cover just outside Nioghalvfjærdssjorden fjorden (Thomsen *et al.* 1997) (fig 12).

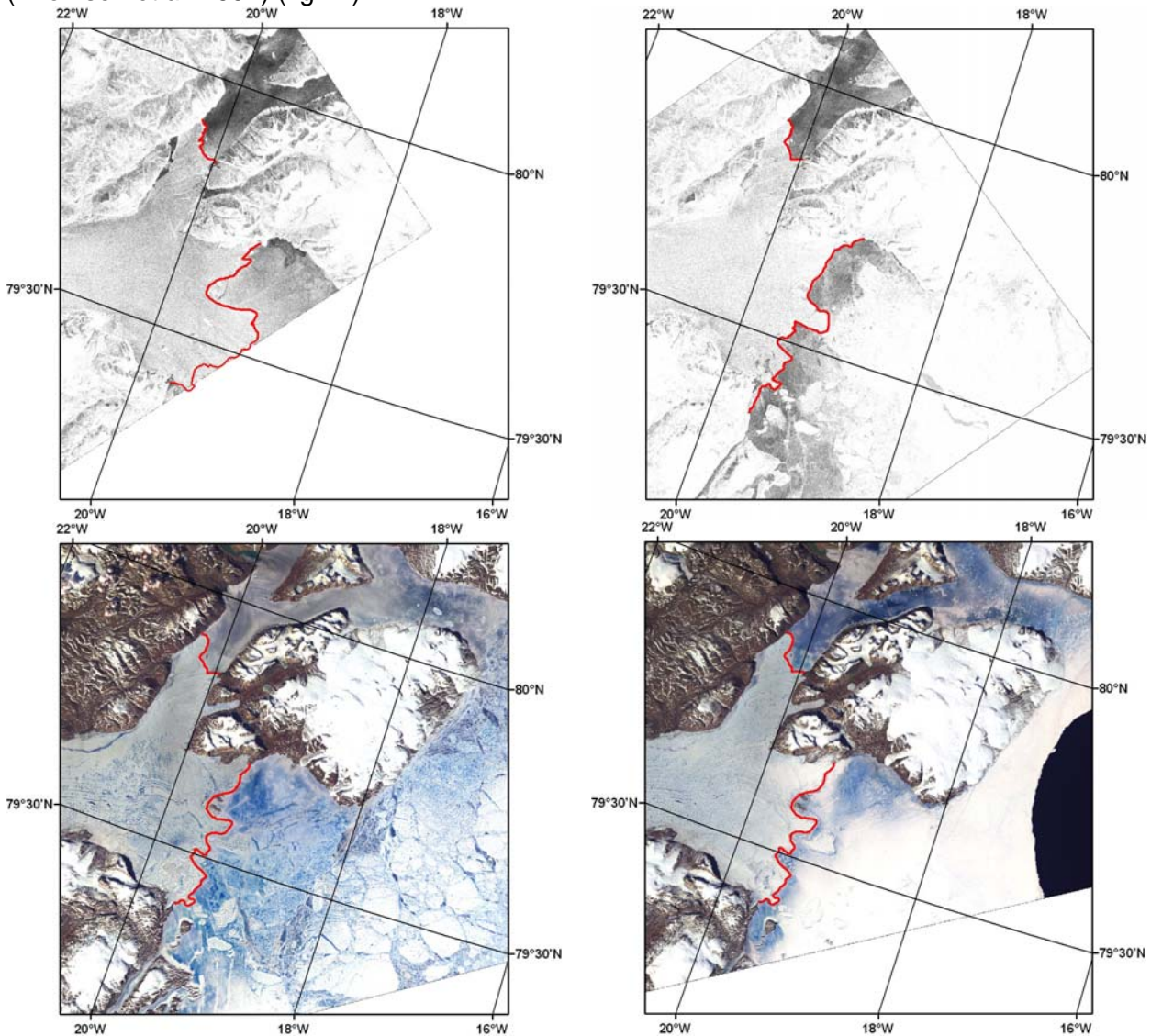


Figure 12. Show 4 images showing the front of the Nioghalvfjærdssjorden Glacier A) ERS from 12 March 1996, B) ERS image from 31 March 1998, C) Landsat image from 2 July 2000 and D) Landsat image from 26 June 2001. All the images show the stable front of the glacier and the permanent presence of sea ice. The Landsat images show the same icebergs in both images which means that they are in the same location for one year.

The same method used in Petremannglacier was applied here to study the surface ice velocity. We started with the Landsat images because they cover a larger area of the glacier than the ERS

SAR images. The dates for these two images are 2 July 2000 and 26 June 2001. We found that the surface velocity is not consistent for the entire glacier; there are clear variations in surface velocity from upper stream to the margin of the glacier tongue. The results show a velocity of 430 m/yr at the front part of glacier (fig 13 the area with a green rectangular), increasing upper stream to a velocity of 990 m/yr (fig 13 the area with violet rectangular).

The middle area in figure 13 (blue rectangular) was used to study the average annual variation surface velocity from 1992 to 1998 using ERS SAR images (Table). Figure 14 shows the annual surface velocity from 1992 to 1998, it seems there was no pattern in increasing or decreasing of the surface velocity in this period, the variation may be due to the different velocity at different areas and also since difference is not big, some part may be due to georeferencing of the images. Thomsen *and others* (1997) carried out a fieldwork on Nioghalvfjærdsfjorden glacier in July – August 1996. They measured the ice flow velocity with GPS; they found a velocity of 560 m/yr at the front part of the glacier and increasing to a maximum velocity of 1240 m/yr in the icefall part of the glacier. The same variation of the velocity was found in this study. They also made preliminary estimate for the mass balance based on a simple ice-flux model using filed data, the result indicate a high melt rate at the bottom of Nioghalvfjærdsfjorden glacier, contribution neglected in models of mass balance of the Greenland ice sheet before.

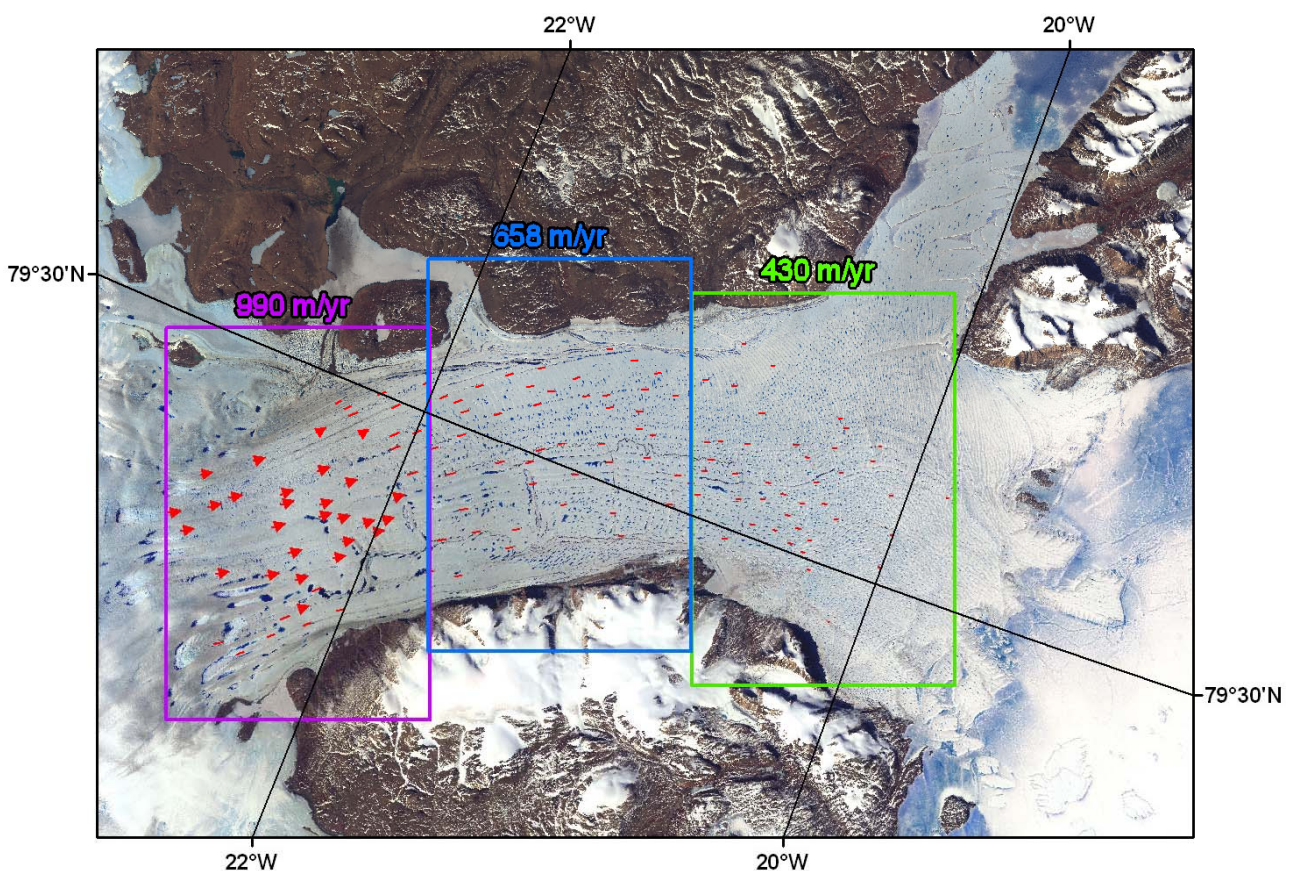


Figure 13. Show a landsat image from 26 June 2000 overlaid by a vector layer represent the surface velocity measured for the period from the 26 June 2000 to 2 July 2001. The colored rectangles show the variation of the surface velocity along the glacier.

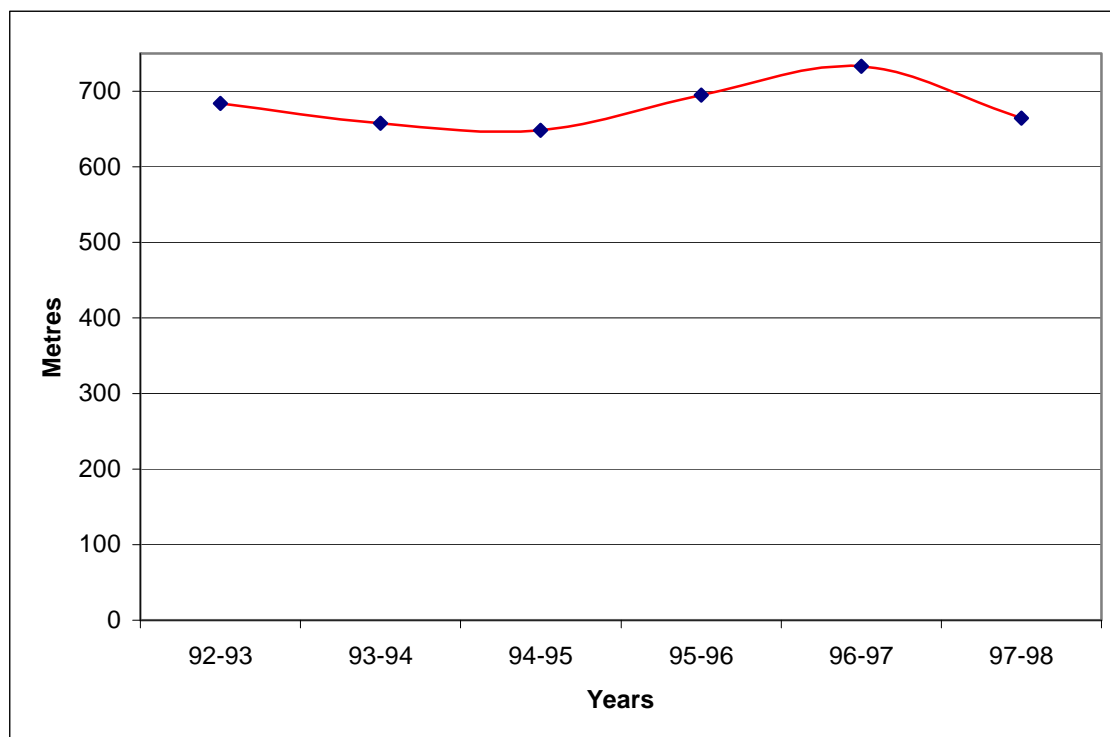


Figure 13. A graph shows the annual average surface velocity for Nioghalvfjærdsfjorden glacier for the period 1992-1998 measured from ERS images.

7. References

- Fichefet, T., C. Poncin, H. Goosse, P. Huybrechts, I. Janssens and H. Le Treut**, 2003: Implications of changes in freshwater flux from the Greenland ice sheet for the climate of the 21st century, *Geophysical Research Letters* **30**, doi: 10.129/2003GL017826.
- Ganapolski, A. and S. Rahmstorf**, 2002: Abrupt glacial climate changes due to stochastic resonance, *Physical Review Letters* **88**, doi: 10.1103/PhysRevLett.88.038501.
- Higgins, A. K., 1991: North Greenland glacier velocities and calf ice production, *Polarforschung* 60(1) 1990, 1-23.
- Huybrechts, P., I. Janssens, C. Poncin and T. Fichefet**, 2002: The response of the Greenland ice sheet to climate changes in the 21st century by interactive coupling of an AOGCM with a thermomechanical ice sheet model, *Annals of Glaciology* **35**, 409-415.
- Huybrechts, P. and J. de Wolde**, 1999: The dynamic response of the Greenland and Antarctic ice sheets to multiple-century climate warming, *Journal of Climate* **12**, 2169-2188.
- Joughin, I., S. Tulaczyk, and others**, 1996: A Mini-Surge On the Ryder Glacier, Greenland, Observed By Satellite Radar Interferometry, *Science* **274**, 228-230.
- Joughin, I., M. Fahnestock**, et al. (1999). "Ice flow of Humboldt, Petermann and Ryder Gletscher, northern Greenland." *JOURNAL OF GLACIOLOGY* **45**(150): 231-241
- Maslowski, W., B. Newton, P. Schlosser, A. Semtner, and D. Martinson**, 2000: Modelling recent climate variability in the Arctic Ocean, *Geophysical Research Letters* **27**, 3743-3746.
- Rahmstorf, S.**, 1995: Bifurcations of the Atlantic Thermohaline Circulation in Response to Changes in the Hydrological Cycle, *Nature* **378**, 145-149.
- Rignot, E.** (1998). "Hinge-line migration of Petermann Gletscher, north Greenland, detected using satellite-radar interferometry." *Journal of Glaciology* **44**(148): 469-476.
- Rignot, E. J., S. Gogineni, I. Joughin and W. Krabill**, 2001: Contribution to the glaciology of northern Greenland from satellite radar interferometry. *Journal of Geophysical Research* **106**, 34,007-34,019.
- Rignot, E.J., S.P. Gogineni, W.B. Krabill, and S. Ekholm**, 1997: North and northeast Greenland ice discharge from satellite radar interferometry, *Science* **276**, 934-937.
- Rignot, E. and P. Kanagaratnam** (2006). "Changes in the velocity structure of the Greenland ice sheet." *SCIENCE* **311**(5763): 986-990.
- Stocker, T.F.**, 2000: Past and future reorganizations in the climate system, *Quaternary Science Review* **19**, 301-319.
- Thomsen, H. H., N. Reeh, O. B. Olesen, C. E. Bøggild, W. Starzer, A. Weidick and A. K. Higgins**, 1997: The Nioghalvfjerdingsfjorden glacier project, North-East Greenland: a study of ice sheet response to climatic change, *Geology of Greenland Survey Bulletin* 179, 95-103.
- Van de Wal, R. S. W., M. Wild and J. De Wolde**, 2001: Short-term volume changes of the Greenland ice sheet in response to doubled CO₂ conditions, *Tellus* **53B**, 94-102
- Whillans, I., J. Bolzan**, et al. (1987). "Velocity of ice streams b and c, Antarctica." *journal of geophysical research-solid earth and planets* **92**(b9): 8895-8902.
- Whillans, I. and Y. Tseng** (1995). "Automatic tracking of crevasses on satellite images." *Cold regions science and technology* **23**(2): 201-214.
- Zwally, H.J., W. Abdalati, T. Herring, K. Larson, J. Saba, and K. Steffen**, 2002: Surface melt-induced acceleration of Greenland ice-sheet flow, *Science* **297**, 218-220.